Dynamics of methane molecules in the mesopores of controlled-pore glass at low temperatures

C. Gutt, B. Asmussen, I. Krasnov, and W. Press
Institut für Experimentelle und Angewandte Physik der Universität Kiel, Olshausenstrasse 40, D-24098 Kiel, Germany

W. Langel*
GKSS Forschungszentrum, Max-Planck-Strasse, D-21502 Geesthacht, Germany

R. Kahn
Laboratoire Léon Brillouin, Commissariat à l'Énergie Atomique, Centre National de la Recherche Scientifique, F-91191 Gif-sur-Yvette Cedex, France

(Received 8 September 1998)

Rotational tunneling of CH_4 molecules in the mesopores of controlled-pore glass with mean diameters of 120 Å and 350 Å has been studied by means of inelastic neutron scattering. The rotational excitation energies of the spherical quantum rotor CH_4 are a sensitive probe of the strength and symmetry of local potentials. The spectra show a superposition of contributions from the partially ordered low temperature phase II of solid CH_4 and from another phase without long range order. This latter phase is attributed to a thin layer with thickness of about 20 Å on the pore walls. A quantitative analysis is performed with a statistical model based on the pocket state formalism. [S0163-1829(99)00413-0]

I. INTRODUCTION

At low temperatures (typically below $T=10$ K), methane molecules in solids are usually treated as spherical top quantum rotors. The rotational tunneling spectra indicate both the symmetry and the magnitude of local potentials. Inelastic neutron scattering (INS) experiments have observed CH_4 molecules in various environments, e.g., CH_4 and its isotopes as substitutional impurities in rare gas crystals,[1] as monolayer adsorbates on graphite[2,3] and MgO,[4,5] and as isolated molecules in clathrate compounds.[6]

In the past, particular attention has been paid to the partially ordered low temperature phase of bulk methane (CH_4-II, see Fig. 1).[7–9] In phase II the methane molecules occupy two different types of sublattices: 25% of the molecules are orientationally disordered and perform almost free rotations in a weak crystalline field of cubic symmetry, while the remaining 75% are orientationally ordered by strong potentials of tetrahedral symmetry (*molecular field*).

These different local symmetries are also reflected in the INS spectra of CH_4-II.[1] The *tunneling lines* at $\hbar\omega = 75$ μeV and at $\hbar\omega = 145$ μeV arise from transitions within the threefold tunnel-split librational ground state of the ordered molecules, while the *free rotor line* at $\hbar\omega = 1.08$ meV corresponds to transitions from the rotational ground state to the first excited rotational state of the disordered molecules. The orientational structure of phase II has been the subject of a large number of theoretical investigations (see Ref. 10 and references therein). These may be classified by the ansatz functions used for the description of the wave function for the CH_4 rotors: (1) the *free-rotor ansatz* and (2) the *pocket-state formalism.*

Calculations based on the *free-rotor ansatz* use an expansion of orientational potential and wave function into free rotor functions (Wigner-D functions).[9] This approach is particularly well-suited for the free rotor molecules in CH_4-II. Predictions by Ozaki *et al.*[11] for the intensity of the $0\rightarrow 1$ transition in INS spectra as a function of momentum transfer Q were found to be in good agreement with experiments using high-resolution neutron spectroscopy.[1]

The *pocket-state formalism*, on the other hand, divides the orientational potential into twelve identically shaped regions (*potential pockets*), which are related by the symmetry operations of the tetrahedral group T. Ansatz functions, which are peaked in single pockets are called *pocket states* (for example δ-functions[12] or Gaussians[13,14] in Euler-angle space).

On the basis of the two limiting cases found in CH_4-II (strongly hindered and almost free rotation) methane molecules may be used as sensitive probes for local potentials also in systems without long-range orientational order. Ex-

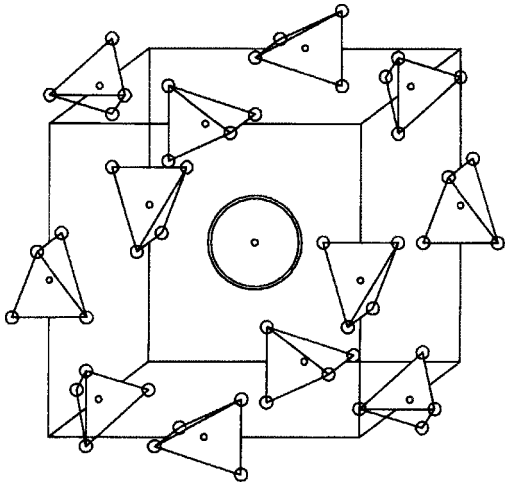

FIG. 1. Orientational structure of the low temperature phase II of solid methane. The circle indicates an orientationally disordered molecule performing almost free rotation, while the other molecules are ordered.

amples are CH_4/krypton mixtures with methane concentrations larger than about 15% (Refs. 16 and 17) and CH_4 in neon matrices.[15] In both cases, broad distributions of excitation energies have been found in the INS spectra, indicating a corresponding distribution of local potentials.

In this paper we present an investigation with neutron spectroscopy of CH_4 molecules as guest molecules in the mesoporous silicate structures of commercially available controlled-pore glass (CPG) with pore diameters $d=120$ Å (CPG-120) and $d=350$ Å (CPG-350). Porous materials are not only interesting because of their technical importance (e.g., in catalysis) but also because they provide a framework for the investigation of the physical properties of solids under the influence of a restricted geometry. Most dynamical studies of guest molecules in porous media concentrate onto the high-temperature regime, where not only rotations but also translations of the center-of-mass may be present and where a classical description is appropriate (e.g., quasielastic neutron scattering). Particularly well investigated are water molecules in different host materials (see, for example, Refs. 20 and 21). An example for quantum rotations in a porous material is hydrogen in Vycor glass.[22,23]

The present work focuses on the low-temperature dynamics ($T \leqslant 10$ K), where no translational diffusion is present and where the rotational transitions of the CH_4 rotors have to be described quantum mechanically. Recently published x-ray diffractograms of krypton and xenon in silicagels with average pore sizes ranging from $d=22$ Å up to $d=100$ Å (Ref. 18) show a clear transition from amorphous solids to structures with long-range translational order with increasing pore size. On the other hand, neutron spectra of methane in the same host materials gave no conclusive evidence for the occurrence of a long-range ordered phase (phase II).[19] In this publication, we will extend the work to larger pore sizes.

This paper is organized as follows: In the next section, we will characterize the sorption behavior of the host materials by showing adsorption/desorption isotherms with CH_4 and we will give the details of the neutron scattering experiment. The INS spectra are presented in Sec. III. In Sec. IV we will describe a statistical model based on the pocket-state formalism for the analysis of the spectra. Section V contains the summary and conclusion.

II. EXPERIMENTAL DETAILS

The controlled-pore glasses were purchased from Sigma Chemicals, St. Louis. In a first step, we have characterized the sorption behavior of CPG-120 (average pore diameter 120 Å) and CPG-350 (average pore diameter 350 Å) by measurements of adsorption-desorption isotherms with methane, in order to determine the conditions necessary for a well-defined filling of the pores. To remove adsorbed water from the pores, the empty CPG-samples were heated up to $T=250$ °C in vacuum before starting the adsorption. The measurements were performed by a volumetric technique, where the sample cell is connected via a valve to a reference volume containing methane gas. Small amounts of gas are dosed in from the reference volume and the equilibrium pressure is recorded by high-precision pressure gauges (MKS–Baratrons). The sorption isotherms of methane at $T=92$ K in CPG-120 are shown in Fig. 2. $p_0=100$ torr is the saturation pressure of methane at $T=92$ K.

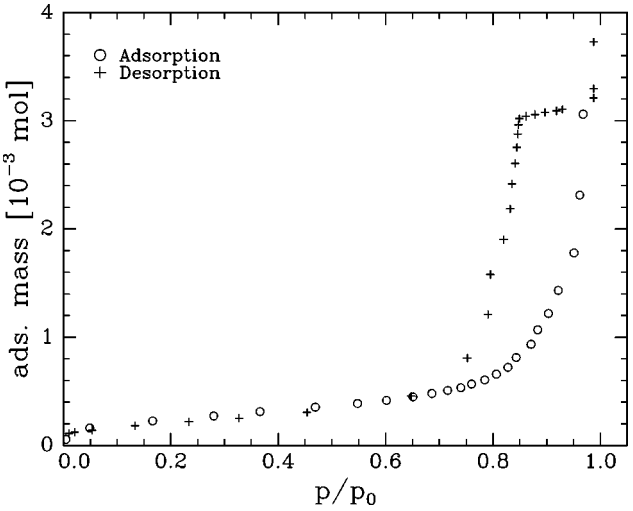

FIG. 2. Adsorption and desorption isotherm of methane condensed in CPG-120 at $T_{Ad}=92$ K. $p_0=100$ torr is the saturation pressure of CH_4 at $T=92$ K.

The almost linear increase of the isotherm at low pressures up to $p/p_0 \sim 0.6$ shows the formation of a multilayer on the inner surfaces of the sample (''BET region,'' see for example Ref. 24). At higher pressures capillary condensation occurs and the amount of adsorbed methane increases strongly. Adsorption and desorption show a strong hysteresis loop (Typ H2, see Ref. 25) which is typical for capillary condensation. The isotherms of methane in CPG-350 (not shown) look very similar to those in Fig. 2, but the hysteresis loop is shifted to higher pressures due to the larger pore radii in CPG-350.

Measurements with inelastic neutron scattering were performed on the neutron time-of-flight spectrometer MIBEMOL on the reactor Orphée of the Laboratoires Léon Brillouin, Saclay. A flat aluminum sample cell of 1 mm thickness was used. The wavelength of the incoming neutrons was $\lambda=5$ Å and 8 Å, respectively. The corresponding energy resolutions at the elastic position were determined by a vanadium standard. For intensity reasons, detectors were grouped together giving nine sum spectra with mean scattering angles $2\theta=40.1°, 47.1°, 55.1°, 63.0°, 75.0°, 89.9°, 105.0°, 121.2°$, and $137.4°$.

As for the thermodynamic measurements described above the empty samples were heated up to $T=200$ °C in vacuum for 12 h until a pressure better than 10^{-4} mbar was achieved. Thereafter the sample cell, which was mounted in a liquid helium cryostat and oriented at an angle of 135° with respect to the incoming neutron beam, was cooled down to $T=92$ K. CH_4 of purity 99.995% was used to load the sample through a heated capillary. This was performed in a two-step process to ensure that the pores are filled with liquid methane without bulk-methane outside the pores.

(1) Methane is filled into the sample cell up to the saturation pressure $p_0=100$ torr at $T=92$ K. This means that not only the pores are filled with liquid methane, but also that bulk-CH_4 exists in the sample cell outside the porous host material.

(2) Methane is partially desorbed down to a relative pressure of $p/p_0 \sim 0.85$. This step removes the bulk methane, but

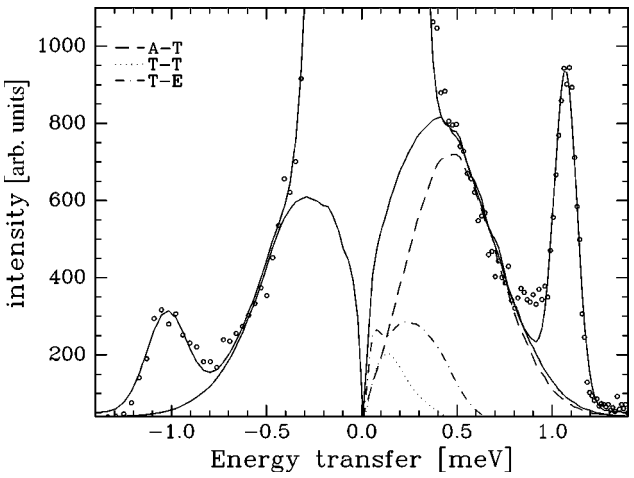

FIG. 3. INS spectrum of CH_4 in CPG-120 at $T=5$ K; time-of-flight spectrometer MIBEMOL, $\lambda=5$ Å. The lines at $\hbar\omega=\pm 1.08$ meV are the free rotor lines of solid CH_4, phase II. The broad distribution between the elastic line and the free rotor lines has been fitted by the model explained in the text. Dashed line: $A\rightarrow T$ transitions; dot-dashed line: $T\rightarrow E$ transitions; dotted line: $T\rightarrow T$ transitions.

the isotherm in Fig. 2 ensures that the pores are still completely filled.

Finally the samples were cooled down to $T=5$ K.

III. INS MEASUREMENTS

Figures 3 and 4 show the INS spectra of CH_4 in CPG-120 and CPG-350 at $T=5$ K ($\lambda=5$ Å). The spectra were obtained by subtracting a scan with the empty CPGs. These empty CPG spectra showed an intense elastic line due to elastic scattering from the host material and the sample container but no indications of inelastic scattering. This makes clear that the inelastic scattering in Figs. 3 and 4 arises solely from the condensed CH_4 molecules. In order to analyze also the Q dependence of the scattered intensity, a standard vanadium calibration and corrections for self-absorption have been performed.

The main feature of both spectra is a superposition of two

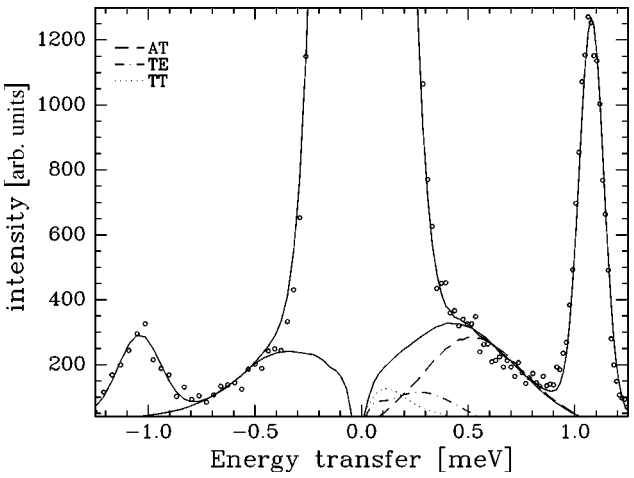

FIG. 4. INS spectrum of CH_4 in CPG-350 at $T=5$ K; time-of-flight spectrometer MIBEMOL, $\lambda=5$ Å.

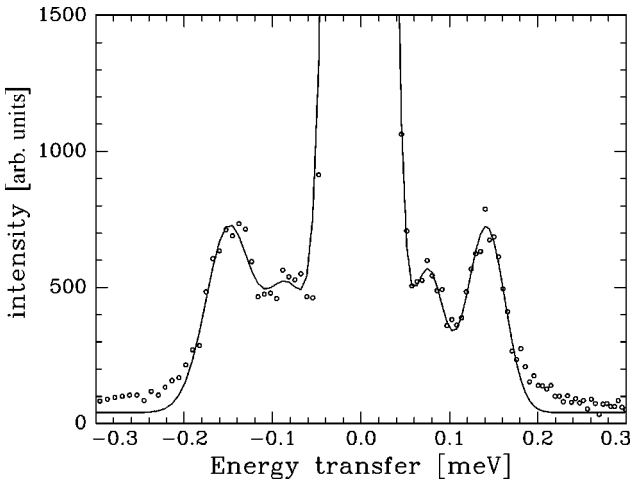

FIG. 5. INS spectrum of CH_4 in CPG-350 at $T=5$ K ($\lambda=8$ Å). The better resolution compared to the scans at $\lambda=5$ Å enables a separation of the tunnelling lines at $\hbar\omega=\pm 77$ μeV and at $\hbar\omega=\pm 145$ μeV from the elastic line.

contributions: (1) At $\hbar\omega=\pm 1.08$ meV the almost free rotor lines of the orientationally ordered phase II are visible. (2) A broad inelastic distribution extends from the elastic line up to the free rotor line. This distribution is attributed to scattering from molecules belonging to a phase without long-range orientational order (we will call this phase I′ in the following).

In order to resolve the tunneling lines of phase II, we have performed a scan with better resolution ($\lambda=8$ Å) with the CH_4/CPG$-$350 system. The spectrum in Fig. 5 shows the A-T and T-E tunneling lines at positions $\hbar\omega_{A\leftrightarrow T}=(145\pm 5)$ μeV and $\hbar\omega_{T\leftrightarrow E}=(77\pm 6)$ μeV in good agreement with values found in phase II of pure methane. A comparison of Figs. 3 and 4 reveals that the relative contribution from phase II to the inelastic signal is much stronger in the system with the larger pores (CPG-350). The quantitative description of the spectra in Figs. 3 and 4 was obtained by fitting the elastic line and the free rotor lines at $\hbar\omega=\pm 1.08$ meV by Gaussians and the broad component by a model, which we will explain in the next section.

In Fig. 6 the measured dependence of the intensity of the free rotor line on momentum transfer Q is plotted together with the theoretical prediction by Ozaki *et al.*[11] on the basis of the free rotor model. The solid curve was obtained by adjusting a normalization constant C in the following expression:

$$S(Q)=C\exp(-\gamma Q^2)p(\hbar\omega_{0\rightarrow 1})f_{01}(Q). \tag{1}$$

$f_{01}(Q)$ is the inelastic structure factor for the $0\rightarrow 1$ transition of the almost free rotors, which has been calculated by Ozaki *et al.* in Ref. 11:

$$f_{01}(Q)=9\times[0.873j_1^2(Qr)+0.0581j_3^2(Qr)+0.0605j_5^2(Qr)]. \tag{2}$$

The j_l are spherical Bessel functions of argument Qr, with $r=1.093$ Å denoting the C-H distance within a CH_4 molecule. j_l with $l\geq 7$ have been neglected in Eq. (2). $\gamma=0.02$ Å^2 has been used for the Debye-Waller factor. The Boltzmann factor

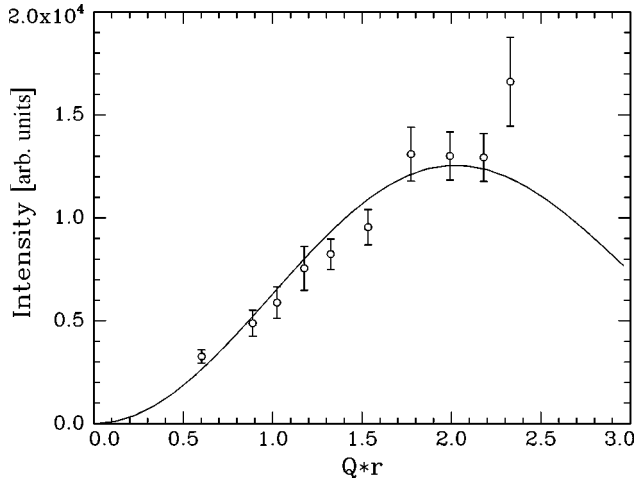

FIG. 6. Dependence of the intensity of the free rotor line in Fig. 5 on momentum transfer Q. The solid line is the theoretical prediction according to Eq. (1) on the basis of the free rotor model by Ozaki *et al.*

$$p(\hbar\omega)=5/Z=5/\left[5+9\exp\left(-\frac{\hbar\omega}{k_BT}\right)\right]. \tag{3}$$

accounts for the decreasing population of the rotational ground state with increasing temperature (note that the degeneracy of the ground state of a free CH_4 rotor is $g=5$ and of the first excited rotational state is $g=9$). A detailed study of the Q dependence of the intensities of both tunnelling lines and free rotor line in pure CH_4-II has been carried out in Ref. 1. For both cases, good agreement of the experiments with the free rotor model has been found.

The elastic line in Figs. 3 and 4 is a superposition of three contributions: (1) Elastic scattering from phase II; (2) tunnelling lines of phase II, which are not resolved from the pure elastic line at that respective energy resolution; (3) elastic scattering from phase I′. On the basis of the free rotor model, a prediction can be made for contributions (1) and (2) as function of Q from the intensity of the free rotor line in Fig. 6. This prediction is shown as solid line in Fig. 7.

Similarly, a prediction of the elastic scattering from molecules in phase I′ may be obtained by the following procedure.

In each of the nine measured spectra, the broad intensity distribution from phase I′ is integrated up to the free rotor energy $\hbar\omega_{\text{free}}=1.31$ meV in the following manner:

$$C_{\mathrm{I}'}=\int_0^{\hbar\omega_{\text{free}}}\frac{S(\hbar\omega)}{p(\hbar\omega)f_{01}(Q(\hbar\omega))}d(\hbar\omega), \tag{4}$$

where the scattered intensity $S(\hbar\omega)d(\hbar\omega)$ within an energy transfer range $[\hbar\omega,\hbar\omega+d(\hbar\omega)]$ is weighted by a Boltzmann factor $p(\hbar\omega)$ and the structure factor $f_{01}(Q)$ of the disordered molecules in CH_4-II [see Eq. (2)]. The notation $f_{01}(Q(\hbar\omega))$ shall indicate that the measurements have been performed as constant 2θ scans rather than as constant Q scans. This causes a slight variation of Q with energy transfer in the single spectra.

$C_{\mathrm{I}'}$ from Eq. (4) is a measure for the number of methane molecules contributing to the signal from phase I′. With the structure factor f_{el} for the elastic line of the free rotors,

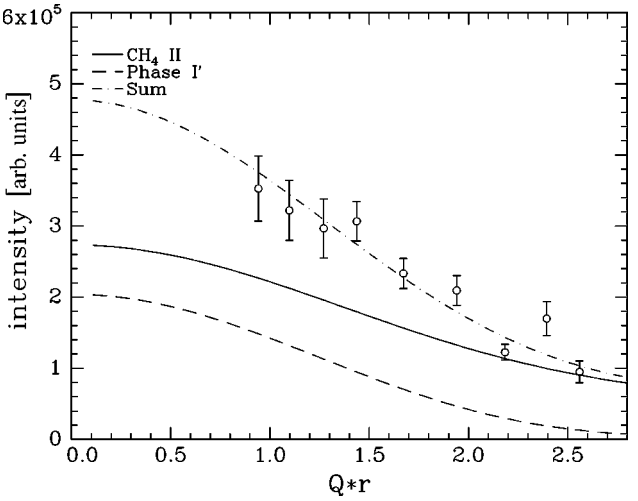

FIG. 7. Q dependence of the elastic line for CH_4 in CPG-120 (see Fig. 4). Circles: experiment; solid line: contribution of pure elastic scattering and tunnelling lines in phase II; dashed line: contribution from phase I′; dot-dashed line: sum of solid and dashed line.

which is proportional to $j_0^2(Qr)$ for small Q values,[11] the Q dependence of the elastic contribution from phase I′ is given by an expression analogous to Eq. (1). This Q dependence is plotted as dashed line in Fig. 7.

The dot-dashed line in Fig. 7 is the sum of the solid line and the dashed line. Hence, it is a prediction for the measured intensity of the elastic line as a function of Q. The good agreement with the measurement (circles) shows that the whole elastic intensity can be explained from the inelastic part of the spectrum. This means that there are no molecules, where the rotation is so strongly hindered that they do not contribute to the inelastic scattering in the accessible energy transfer range.

The normalization constants C and $C_{\mathrm{I}'}$ are, as already mentioned, a measure for the number of molecules in the two phases I′ and II. From their numerical values, we have have obtained a ratio 1:1 in CPG-120 and a ratio 1:2 in CPG-350 for the number of molecules in phase I′ to the number of molecules in phase II.

IV. QUANTITATIVE ANALYSIS OF THE SCATTERING FROM PHASE I′

The neutron spectra, which were presented in the previous section are characterized by the superposition of two contributions: scattering from an almost unperturbed phase II and scattering from another phase (we call this phase I′) without long-range orientational order. In this section, we derive the model used for the quantitative analysis of the signal from phase I′ in the INS spectra. The basic idea of this model is to calculate the intensity distribution (as function of energy transfer) in the INS spectra from a properly chosen probability distribution for the tunnel matrix elements.

Within the framework of the pocket-state formalism, each CH_4 tetrahedron may be characterized by seven overlap matrix elements, which are a measure for the overlap of wave functions in different pocket states:[10] H_x, H_y, H_z correspond

to 180° overlap matrix elements (this means they describe the overlap between wave functions for orientations of the CH_4 tetrahedron, which may be transformed into each other by a 180° rotation about a twofold symmetry axis) and h_1, h_2, h_3, h_4 correspond to 120° overlap matrix elements. Site symmetry reduces the number of independent matrix elements. For tetrahedral site symmetry ($\bar{4}2m$), as in the case of the ordered molecules in CH_4-II, all 120° overlap matrix elements are equal.

For describing the rotations in a disordered phase, we make the following assumptions:

180° overlap matrix elements are neglected, i.e., $H_x = H_y = H_z = 0$.

120° overlap matrix elements are randomly distributed according to a Gaussian distribution around a mean value h_0. This accounts for a statistical distribution of local potentials of low symmetry.

$$f(h_i) \sim \exp\left(-\frac{(h_i - h_0)^2}{2\delta^2} \right), \quad i = 1, \ldots, 4. \tag{5}$$

In the case of a low-symmetry potential, the librational ground state of a CH_4 molecule splits into five sublevels (*tunnel levels*), which are classified according to their symmetry $\Gamma (\Gamma = A, T_1, T_2, T_3, E)$ with respect to rotations of the molecule (see Fig. 8). The energies of the A level and the E level are given by[10]

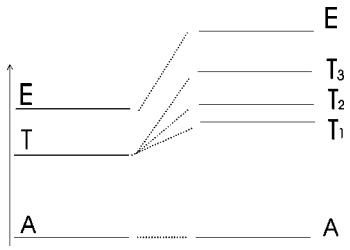

FIG. 8. Tunnel splitting of the librational ground state of a CH_4 molecule in a field of tetrahedral symmetry (left) and in a field of low symmetry (right). The rotational levels are labelled according to their symmetry with respect to the tetrahedral group T.

$$E_A = D - 2(h_1 + h_2 + h_3 + h_4), \tag{6}$$

$$E_E = D + h_1 + h_2 + h_3 + h_4. \tag{7}$$

D denotes the diagonal element of the 12×12 Hamilton matrix. The energies $E_{T_1}, E_{T_2}, E_{T_3}$ of the T levels are obtained as the eigenvalues of the matrix:[10]

$$\hat{H}_T = \begin{pmatrix} D & -h_1 - h_2 + h_3 + h_4 & -h_1 + h_2 - h_3 + h_4 \\ -h_1 - h_2 + h_3 + h_4 & D & +h_1 - h_2 - h_3 + h_4 \\ -h_1 + h_2 - h_3 + h_4 & +h_1 - h_2 - h_3 + h_4 & D \end{pmatrix}.$$

Transitions $\Gamma_i \rightarrow \Gamma_f$ between the five levels in Fig. 8 show up in the neutron spectrum at energy transfers $\Delta(\Gamma_i \rightarrow \Gamma_f) = E_{\Gamma_f} - E_{\Gamma_i}$. Since transitions $A \leftrightarrow E$ cannot be induced by a neutron, there is a total of nine energy transfers with $\Delta > 0$ and nine corresponding transitions with $\Delta < 0$ in addition to the elastic scattering from transitions with $\Gamma_i = \Gamma_f$. For a particular choice of h_0 and δ, an INS spectrum is simulated by a Monte Carlo procedure.

(1) A set (denoted by a number k) of four matrix elements $h_1^k, h_2^k, h_3^k, h_4^k$ is randomly chosen from the distribution in Eq. (5).

(2) The energies $E_A^k, E_{T_1}^k, E_{T_2}^k, E_{T_3}^k, E_E^k$ are calculated from Eqs. (6), (7) and by diagonalizing matrix $\hat{H}$. This yields the set of $9 \times 2 = 18$ transition energies $\Delta(\Gamma_i \rightarrow \Gamma_f)$ within the fivefold tunnel-split librational ground state.

(3) Each *molecule k* contributes to the neutron spectrum at the energy transfers $\Delta(\Gamma_i \rightarrow \Gamma_f)$ with the weight

$$w(\Delta(\Gamma_i \rightarrow \Gamma_f)) = p_i(T) \times I(\Gamma_i \rightarrow \Gamma_f), \tag{8}$$

where p_i is the population of the respective ground state Γ_i, calculated from a Boltzmann distribution for the sample temperature of $T = 5$ K. $I(\Gamma_i \rightarrow \Gamma_f)$ denotes the probability of a transition $\Gamma_i \rightarrow \Gamma_f$. These transition probabilities depend on the values of the h_i and were calculated according to the formalism described in Ref. 10. More details are given in the Appendix.

Steps (1)–(3) are repeated typically 10^6 times and the INS spectrum finally is obtained by summing up all $w(\Delta)$ in Eq. (8).

The broad distribution of scattered intensities in the INS spectra (Figs. 3 and 4) has been fitted by variation of the model parameters h_0 and δ [see Eq. (5)]. $h_0 = 0.065 \pm 0.005$ meV and $\delta = 0.04 \pm 0.01$ meV were found for CH_4 in CPG-120. The corresponding values for CH_4 in CPG-350 are identical within the error bars. The fits (lower solid lines in Fig. 3 and in Fig. 4) agree well with the measurements. Figure 3 additionally shows separately the contributions from $A \rightarrow T_i$ transitions (dashed line), $T_i \rightarrow E$ transitions (dot-dashed line), and $T_i \rightarrow T_j$ transitions (dotted line).

V. SUMMARY AND CONCLUSION

The INS measurements have shown the coexistence of a *core* of an almost unperturbed phase II of solid methane with a phase without long range orientational order (phase I′). The signal from the latter phase is similar to what has been observed with CH_4 in silicagels with pore diameters $d \leq 60$ Å.[19] The analysis of the elastic intensity has proven that there are no methane molecules present, which contrib-

TABLE I. Relative (powder averaged) intensities $I(\Gamma_i \rightarrow \Gamma_f)$ of the transitions $\Gamma_i \rightarrow \Gamma_f$ within the tunnel-split librational ground state of a CH_4 molecule in a potential of tetrahedral symmetry (i.e., $h_1=h_2=h_3=h_4$). The Q dependence is determined by the spherical Bessel function $j_0(\sqrt{8/3}QR)$.

	A	T_1	T_2	T_3	E
A	$135(1+3j_0)$	$45(1-j_0)$	$45(1-j_0)$	$45(1-j_0)$	0
T_1	$45(1-j_0)$	$27(1+3j_0)$	$27(1-j_0)$	$27(1-j_0)$	$36(1-j_0)$
T_2	$45(1-j_0)$	$27(1-j_0)$	$27(1+3j_0)$	$27(1-j_0)$	$36(1-j_0)$
T_3	$45(1-j_0)$	$27(1-j_0)$	$27(1-j_0)$	$27(1+3j_0)$	$36(1-j_0)$
E	0	$36(1-j_0)$	$36(1-j_0)$	$36(1-j_0)$	0

ute neither to the signal from phase II nor to that from phase I′. Therefore the ratio of the inelastic intensity from the two phases is a direct measure for the relative number of molecules in the unperturbed phase II. We assume that the molecules in phase I′ form a *thin film* on the pore walls and we furthermore assume a spherical shape of the cavities with diameters of 120 Å in CPG-120 and of 350 Å in CPG-350, respectively. Under these two assumptions it is possible to calculate the thickness of the film. In both cases, a thickness of $d=20\pm5$ Å has been calculated. We want to mention that the assumption of two well separated phases of the condensate is an approximation, which neglects relaxation processes at the interface between phase I′ and phase II. It is very likely that the real transition from the disordered phase I′ to the (partially) ordered phase II occurs continuously with increasing distance from the pore walls. Additionally, no separate behavior of the molecules on the pore walls (BET-range) has been taken into account.

A model based on a statistical distribution of tunnel matrix elements provides a quantitative description of the scattered intensity from phase I′. From the average matrix element $h_0=0.065$ meV one may obtain the average strength of the orientational potential from the following consideration: Hüller and Voll[13,14] have calculated the dependence of the energy $\hbar\omega_{AT}$ of the $A \rightarrow T$ transition of a tetrahedron in a potential of tetrahedral symmetry on the magnitude of the orientational potential:

$$\hbar\omega_{AT}=E_{\text{free}}\exp\left(-\frac{V^2}{2\Gamma^2}\right). \tag{9}$$

$E_{\text{free}}=1.31$ meV is the energy of the first excited rotational state of the completely free CH_4 rotor. Identifying $\hbar\omega_{AT}$ with the average energy of the T levels $\hbar\omega_{AT}=8h_0$,[10] and using the numerical values $h_0=0.065$ meV and $\Gamma=10.15$ meV, one obtains an average $V=14.3$ meV. Here we have used the same numerical value for Γ as for the description of the INS spectra of CH_4 in neon matrices. For a more detailed discussion the reader is referred to Ref. 15. $V=14.3$ meV for the potential strength is similar to values, which have been found for methane in silicagels with pore diameters $d\leqslant 60$ Å.[19] In these cases, only contributions from a disordered phase were observed and no indications for a phase II showed up in the INS spectra.

Future structural investigations (mainly with small angle neutron scattering) will focus on the development of more realistic models for geometry and topology of the mesopores. Further inelastic neutron scattering experiments are aimed at the melting behavior of the methane condensates.

TABLE II. Matrix elements $M(T_i,m_i;T_f,m_f)$ [see Eq. (10)] for a CH_4 molecule in a potential of tetrahedral symmetry.

Γ		T_1			T_2			T_3		
	m	$+1$	0	-1	$+1$	0	-1	$+1$	0	-1
T_1	$+1$	$-bG_A$	eG_A	0	bG_Z	$-eG_Z$	0	bG_Y	$-eG_Y$	0
	0	eG_A	0	eG_A	$-eG_Z$	0	$-eG_Z$	$-eG_Y$	0	$-eG_Y$
	-1	0	eG_A	bG_A	0	$-eG_Z$	$-bG_Z$	0	$-eG_Y$	$-bG_Y$
T_2	$+1$	bG_Z	$-eG_Z$	0	$-bG_A$	eG_A	0	bG_X	$-eG_X$	0
	0	$-eG_Z$	0	$-eG_Z$	eG_A	0	eG_A	$-eG_X$	0	$-eG_X$
	-1	0	$-eG_Z$	$-bG_Z$	0	eG_A	bG_A	0	$-eG_X$	$-bG_X$
T_3	$+1$	bG_Y	$-eG_Y$	0	bG_X	$-eG_X$	0	$-bG_A$	eG_X	0
	0	$-eG_Y$	0	$-eG_Y$	$-eG_X$	0	$-eG_X$	eG_X	0	eG_X
	-1	0	$-eG_Y$	$-bG_Y$	0	$-eG_X$	$-bG_X$	0	eG_X	bG_X

TABLE III. Relative (powder averaged) intensities $I(\Gamma_i \rightarrow \Gamma_f)$ of the transitions $\Gamma_i \rightarrow \Gamma_f$ within the five-fold tunnel-split librational ground state of a CH_4 molecule in a low-symmetry potential for a particular choice of the tunnel matrix elements ($h_1, h_2 = 1.1h_1, h_3 = 0.9h_1, h_4 = 0.95h_1$). The intensities of transitions $A \rightarrow T_i$ and $T_i \rightarrow E$ do not depend on the numerical values of the matrix elements h_i and are therefore identical with those in Table I.

	A	T_1	T_2	T_3	E
A	$135(1+3j_0)$	$45(1-j_0)$	$45(1-j_0)$	$45(1-j_0)$	0
T_1	$45(1-j_0)$	$60.7+47.3j_0$	$14.9-14.9j_0$	$5.4-5.4j_0$	$36(1-j_0)$
T_2	$45(1-j_0)$	$14.9-14.9j_0$	$47.9+60.1j_0$	$18.2-18.2j_0$	$36(1-j_0)$
T_3	$45(1-j_0)$	$5.4-5.4j_0$	$18.2-18.2j_0$	$57.3+50.7j_0$	$36(1-j_0)$
E	0	$36(1-j_0)$	$36(1-j_0)$	$36(1-j_0)$	0

ACKNOWLEDGMENTS

This work was supported by *Deutsche Forschungsgemeinschaft* under Contract No. PR325/7-1.

APPENDIX

In the following, we briefly describe the formalism for calculating the transition probabilities $I(\Gamma_i \rightarrow \Gamma_f)$ used in Eq. (8). The general formalism is presented in detail in Ref. 10. Table I contains the relative intensities of the transitions $\Gamma_i \rightarrow \Gamma_f$ calculated with the pocket-state formalism for the ordered molecules in CH_4 (i.e., $h_1 = h_2 = h_3 = h_4$).[10] Their dependence on momentum transfer Q is given by the spherical Bessel function $j_0(\sqrt{8/3}Qr)$, where $r = 1.09$ Å is the C-H distance within a CH_4 molecule (see Table I). For a powder sample, the intensities of transitions $A \rightarrow T_i$ and of transitions $T_i \rightarrow E$ are independent of the matrix elements h_i within the pocket-state formalism. The intensities of transitions $T_i \rightarrow T_j$, however, do depend on the numerical values of the h_i (more accurately on their differences) and may be obtained from the following sum:

$$\tilde{I}(T_i \rightarrow T_f) = \sum_{m_i=-1}^{+1} \sum_{m_f=-1}^{+1} |M(T_i, m_i; T_f, m_f)|^2. \quad \text{(A1)}$$

The $M(T_i, m_i; T_f, m_f)$ are the elements of a 9×9 matrix given in Table II for the case of a CH_4 molecule in a potential of tetrahedral symmetry (ordered molecules in CH_4-II). We have used the following abbreviations:

$$b = \frac{1}{2}, \quad e = \frac{1}{\sqrt{2}}, \quad G_\gamma = \exp(i\vec{Q}\vec{r}_\gamma), \quad \text{(A2)}$$

$$G_A = \frac{1}{2}\sum_{\gamma=1}^{4} G_\gamma, \quad G_X = \frac{1}{2}(G_1 - G_2 - G_3 + G_4), \quad \text{(A3)}$$

$$G_Y = \frac{1}{2}(G_1 - G_2 + G_3 - G_4), \quad G_Z = \frac{1}{2}(G_1 + G_2 - G_3 - G_4). \quad \text{(A4)}$$

$\vec{r}_\gamma$ denotes the position of proton $\gamma(\gamma = 1,2,3,4)$ in a CH_4 molecule within a space-fixed reference frame. Finally, a powder average has to be performed, which is readily done with (see Ref. 12)

$$\langle G_\lambda G_\mu^* + G_\lambda^* G_\mu \rangle = \begin{cases} 2 & : \quad \lambda = \mu \quad \lambda, \mu = 1,2,3,4 \\ 2j_0(\sqrt{8/3}Qr) & : \quad \lambda \neq \mu \quad \lambda, \mu = 1,2,3,4. \end{cases} \quad \text{(A5)}$$

This procedure yields the intensities $I(\Gamma_i \rightarrow \Gamma_f)$ as function of momentum transfer Q (see Table I), which are used in Eq. (8).

As mentioned above, the intensities of the $T_i \rightarrow T_j$ transitions depend on the particular values of the tunnel matrix elements h_1, h_2, h_3, h_4. The matrix $\hat{M}'(h_1, h_2, h_3, h_4)$, which determines for an arbitrary set of matrix elements h_i the intensities according to Eq. (A1), is obtained from the matrix $\hat{M}(h_1 = h_2 = h_3 = h_4)$ in Table II by

$$\hat{M}' = \hat{R}^T \hat{M} \hat{R}. \quad \text{(A6)}$$

The 9×9 matrix $\hat{R}$ may be written as

$$\hat{R} = \begin{pmatrix} R_{11}\hat{E} & R_{12}\hat{E} & R_{13}\hat{E} \\ R_{21}\hat{E} & R_{22}\hat{E} & R_{23}\hat{E} \\ R_{31}\hat{E} & R_{32}\hat{E} & R_{33}\hat{E} \end{pmatrix}, \quad \text{(A7)}$$

with $\hat{E}$ being the 3×3 unity matrix. The R_{ij} are the elements of the 3×3 matrix, which diagonalizes the 3×3 matrix $\hat{H}_T$ in Sec. III. As an example, we show in Table III the intensities calculated to the described procedure for a set of matrix elements with $h_1, h_2 = 1.1h_1, h_3 = 0.9h_1$, and $h_4 = 0.95h_1$.

*Present address: Institut für Physikalische Chemie, Soldtmannstrasse, D-17487 Greifswald, Germany.
[1] B. Asmussen, M. Prager, W. Press, H. Blank, and C.J. Carlile, J. Chem. Phys. **97**, 1332 (1992); B. Asmussen, D. Balszunat, W. Press, C.J. Carlile, and H. Büttner, *ibid.* **103**, 221 (1995).
[2] M.V. Smalley, A. Hüller, R.K. Thomas, and J.W. White, Mol. Phys. **44**, 533 (1981).
[3] R.P. Humes, M.V. Smalley, T. Rayment, and R.K. Thomas, Can. J. Chem. **66**, 557 (1988).
[4] J.Z. Larese, J.M. Hastings, L. Passell, D. Smith, and D. Richter, J. Chem. Phys. **95**, 6997 (1991).
[5] J.Z. Larese, B. Asmussen, M.A. Adams, C.J. Carlile, D. Martin, and M. Ferrand, Physica B **226**, 221 (1996).
[6] A. Schröder-Heber, B. Asmussen, W. Press, H. Blank, and H. Gies, Mol. Phys. **82**, 857 (1994).
[7] H.M. James and T.A. Keenan, J. Chem. Phys. **31**, 12 (1959).
[8] W. Press, J. Chem. Phys. **56**, 2597 (1972).
[9] T. Yamamoto, Y. Kataoka, and K. Okada, J. Chem. Phys. **66**, 2701 (1977).
[10] W. Press, *Single Particle Rotations in Molecular Crystals*, Springer Tracts in Modern Physics Vol. 92 (Springer-Verlag, Berlin, 1981).
[11] Y. Ozaki, Y. Kataoka, and T. Yamamoto, J. Chem. Phys. **73**, 3442 (1980).
[12] A. Hüller, Phys. Rev. B **16**, 1844 (1977).
[13] A. Hüller and J. Raich, J. Chem. Phys. **71**, 3851 (1979).
[14] G. Voll and A. Hüller, Can. J. Chem. **66**, 925 (1988).
[15] M. Prager, B. Asmussen, and C.J. Carlile, J. Chem. Phys. **100**, 247 (1994).
[16] S. Grondey, M. Prager, W. Press, and A. Heidemann, J. Chem. Phys. **85**, 2204 (1986).
[17] S. Grondey, M. Prager, and W. Press, J. Chem. Phys. **86**, 6465 (1987).
[18] B. Schäfer, B. Balszunat, W. Langel, and B. Asmussen, Mol. Phys. **89**, 1057 (1996).
[19] D. Balszunat, B. Asmussen, G. Coddens, and M. Ferrand, Physica B **226**, 184 (1996).
[20] J.D.F. Ramsay and C. Poinsignon, Langmuir **3**, 320 (1987).
[21] M.C. Bellissent-Funel, S.H. Chen, and J.M. Zanotti, Phys. Rev. E **51**, 4558 (1995).
[22] J. De Kinder, A. Bouwen, and D. Schoemaker, Phys. Rev. B **52**, 15 872 (1995)
[23] A.W. Adamson, *Physical Chemistry of Surfaces* (Wiley, New York, 1990).
[24] S. Brunauer, P.H. Emmett, and E. Teller, J. Am. Chem. Soc. **60**, 309 (1938).
[25] J.H. Block, A.M. Bradshaw, P.C. Gravelle, J. Haber, R.S. Hansen, M.W. Roberts, N. Sheppard, and K. Tamaru, Pure Appl. Chem. **62**, 2297 (1990).